Multiplex Digital MicroRNA Detection Using Cross-Inhibitory DNA Circuits

Yannick Rondelez and Guillaume Gines*

Cite This: *ACS Sens.* 2020, 5, 2430−2437

Read Online

ACCESS | 📊 Metrics & More | 📖 Article Recommendations | 🆂ℹ Supporting Information

ABSTRACT: Ubiquitous post-transcriptional regulators in eukaryotes, microRNAs are currently emerging as promising biomarkers of physiological and pathological processes. Multiplex and digital detection of microRNAs represents a major challenge toward the use of microRNA signatures in clinical settings. The classical reverse transcription polymerase chain reaction quantification approach has important limitations because of the need for thermocycling and a reverse transcription step. Simpler, isothermal alternatives have been proposed, yet none could be adapted in both a digital and multiplex format. This is either because of a lack of sensitivity that forbids single molecule detection or molecular cross-talk reactions that are responsible for nonspecific amplification. Building on an ultrasensitive isothermal amplification mechanism, we present a strategy to suppress cross-talk reactions, allowing for robust isothermal and multiplex detection of microRNA targets. Our approach relies on target-specific DNA circuits interconnected with DNA-encoded inhibitors that repress nonspecific signal amplification. We demonstrate the one-step, isothermal, digital, and simultaneous quantification of various pairs of important microRNA targets.

KEYWORDS: *multiplex assay, DNA circuit, microRNA, digital droplet detection, isothermal amplification*
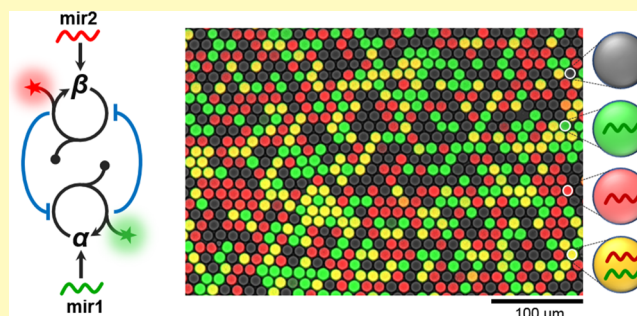
The ultrasensitive detection of nucleic acids traditionally employs exponential amplification. Polymerase chain reaction (PCR) is undoubtedly the most widespread nucleic acid amplification technique, displaying an impressive sensitivity, in many cases down to a single molecule and being compatible with recent digital readout formats. Still, it has a number of issues, including the necessity of thermocycling and the fact that it amplifies the target sequence itself, which leads to a high risk of sample-to-sample carry-over contamination. Several isothermal alternatives have been explored to address these problems.[1] These include rolling circle amplification,[2,3] loop-mediated isothermal amplification,[4] strand displacement amplification,[5−7] recombinase polymerase amplification,[8,9] or exponential amplification reaction (EXPAR).[10] These enzymatic systems provide robust amplification at a constant, relatively low temperature, and some can be designed to avoid amplification of the target sequence. Although their sensitivity in bulk is typically not as good as that of PCR, many of them have been demonstrated in a digital format.[11−15]

An important feature of the various nucleic acid quantification approaches is whether or not they can be multiplexed. Simultaneous readout for the quantification of several target molecules (multiplexing) is critical to reduce the experimental load, to minimize the quantity of the starting material, or to perform internal normalization. Multiplex assays can be categorized as supported and in-solution assays.

Supported assays refer to microarrays or suspension arrays where indexed spatial locations are functionalized by specific probes.[16−18] Because the same signal (e.g., green fluorescence) can be used for all targets, this strategy presents high multiplexing capabilities (up to hundreds of different targets). However, such assays require surface modification,[19] preamplification, or the optimization of the chemistry to work in a heterogeneous environment.[20,21] Importantly, array-based systems are difficult to convert to a digital format, and for this reason, they are limited in quantitativity and sensitivity.

In contrast, in-solution multiplexing approaches are compatible with the digital readout,[22,23] but require individual chemical sensors (e.g., primers or templates) and detectors (e.g., spectrally, temporally, or intensity-resolved fluorescent probes) for each target.[22,24−26] This increases the chemical complexity and possibly brings cross-reactivity issues. For example, multiplex PCR requires careful design of orthogonal primers and optimization of thermocycling conditions to avoid the emergence of primer dimers or cross-amplification
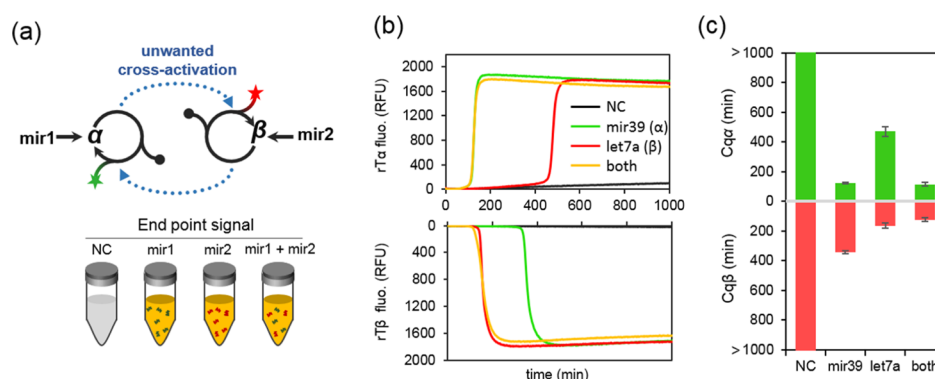
Figure 1. Cross-talk reactivity between isothermal amplification reactions prevents multiplex quantification. (a) Two positive-feedback reactions are designed to sense the presence of two different microRNAs (mir1 and mir2). However, the competition for catalytic resources leads to unwanted cross-activation, where both switches are ultimately triggered whenever at least one of the targets is present, leading to false-positive end-point signals for both green (probe rTα) and red (probe rTβ) colors (=orange color). (b) Amplification curves of two combined switches α and β triggered with 0 or 10 pM of mir39 and let7a microRNA, respectively. When spiked with only one of the two microRNA (green and red curves), we observe that the nontriggered switch self-starts shortly after the triggered switch. (c) Amplification time (Cq) of a triplicate experiment.

(especially when some of the targets are closely related). In addition, the multiple concurrent amplification reactions compete for chemical resources (i.e., enzymes), thus affecting the quantification of the target concentration using real-time methods. This last issue is circumvented by transferring the test to a digital format, where the amplification mixture is partitioned into a large number of microscopic compartments before amplification.[27] This is because, first, concentrations are inferred from the end-point fraction of positive compartments, which is robust to kinetic perturbations, and second, because each potential target gets its own compartment; therefore, the opportunities for cross-reactivity decreases.

In the present study, we start from a solution-phase isothermal approach to detect microRNA, which is based on signal amplification using reprogrammable molecular circuits. This procedure has recently been adapted in a digital format,[28] and we wished to explore its multiplexing potential. We first show that molecular cross-talks generate unwanted interferences between multiplexed detection channels. These issues seem critical enough to hamper direct detection of multiple species, especially when attempting to quantify weak molecular signals. Thus, we developed a dedicated tetrastable molecular circuit, where designed inhibition reactions between each switch avert cross-talks. This circuit allows us to establish a duplex droplet digital format, which provides the first isothermal demonstration of calibration-free absolute quantification of two microRNAs simultaneously. More generally, our strategy opens a route to build more functional diagnostic approaches in nucleic acid testing, using rational building of molecular circuits.

■ RESULTS AND DISCUSSION

Cross-Reactivity between Individual Switches Prevents Multiplexing. We started by assessing the possibility of multiplexing isothermal exponential DNA amplification reactions targeting microRNA (Figure 1). To detect minute quantities of these short sequences, we have reported a nickase−polymerase−exonuclease system whose sensitivity has been boosted (limit of detection < 10 fM), thanks to a leak-absorption mechanism, which counterbalances nonspecific amplification caused by primer-independent polymerization.[28] In this system, a typical singleplex amplification mixture is composed of four DNA templates, each designed to perform a specific function: a conversion template (cT, e.g., mir39toα), which, upon hybridization to its cognate microRNA target (e.g., mir39), linearly produces a 12-mer oligonucleotide trigger (e.g., α) using polymerization/nicking cycles. The trigger, in turn, stimulates a bistable amplification switch made of an amplification template (aT, e.g., aTα) and a pseudotemplate (pT, e.g., pTα). The aT exponentially amplifies the trigger strand. The pT is responsible for prevention of nonspecific amplification observed in traditional EXPAR systems[29−31] by deactivating a certain fraction of the α strands stemming from leaky reactions on the aT.[32] The pT binds its input trigger, to which it templates the addition of a few nucleotides at the 3′ extremity. Finally, a reporting template (e.g., rTα) modified with a quencher/fluorophore pair is designed to bind the trigger strands, generating a specific fluorescence signal. We designed two circuits, sensing the presence of mir39 and let7a, respectively. The first circuit uses sequence α for signal amplification, and the second circuit uses a different sequence (β), so that the two systems are orthogonal at the sequence level. Figure 1b presents the amplification time traces recorded in the presence (10 pM) or absence of the targets. In the absence of both targets (negative control, "NC"), no amplification is observed (time recorded = 1000 min), whereas the presence of both targets elicits a response in around 100 min. This proves the efficacy of the leak-absorption mechanism to avoid nonspecific amplification, even when multiple switches are present in the same mixture. However, when only mir39 is spiked in the mixture, we observed that the associated switch is indeed triggered, but it is shortly followed by the unstimulated switch. The same observation is made for let7a. This suggests the existence of a cross-talk mechanism between the two switches, causing false-positive detection. Consequently, it appears impossible to perform accurate real-time measurements of two targets in a single tube.

The existence of global, sequence-independent cross-talks was indeed noted earlier. It was also suggested that these cross-talks result from enzyme sequestration.[33,34] We therefore attempted to remove this effect by optimizing component concentration. We observed in particular that the nonspecific amplification effect was sensitive to the concentration of the nicking enzyme Nb.BsmI, with less enzyme leading to faster false start (Figure S1). This led us to speculate that the first
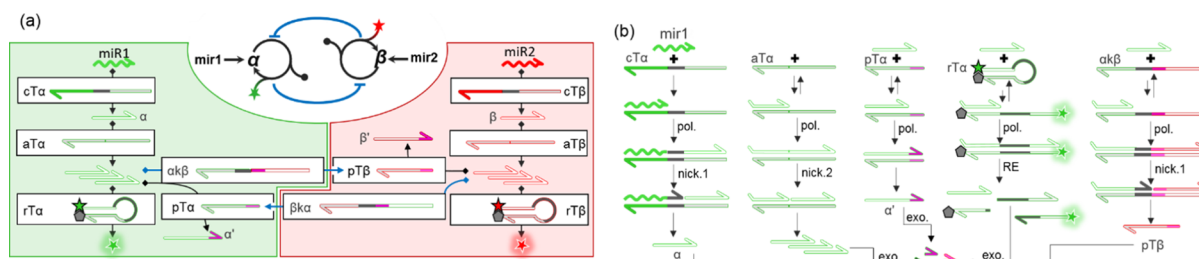
Figure 2. Tetrastable system built from two cross-inhibitory bistable switches. (a) Schematic of the tetrastable DNA circuit. Two microRNA-sensing circuits (cT, aT, pT, and rT) are interconnected by kT $\alpha k\beta$ and $\beta k\alpha$, which repress unwanted cross-activation. (b) Detailed mechanism of the five kinds of templates (pol. = Vent(exo-), nick. 1 = Nt.BstNBI, nick. 2 = Nb.BsmI, RE = BsmI, and exo. = ttRecJ). cTs convert the complementary microRNA target to a signal strand (α or β). Autocatalytic templates (aTs) exponentially amplify the signal strands. pTs, by deactivating a fraction of signal strands, suppress background amplification stemming from biochemical noise. Reporting templates (rTs) transduce the molecular signal (α or β) to a detectable fluorescence signal (green = Oregon green fluorophore, red = Atto633 fluorophore). From the α or β strands, killer templates (kTs) produce pTs of the opposite switch, mitigating unspecific cross-talks. All produced strands are continuously degraded by the exonuclease to maintain the system dynamics and avoid system poisoning by the accumulation of DNA strands. Only one half of the tetrastable circuit is represented here, the second half being obtained by substituting α by β and conversely.

amplification induces the sequestration of this enzyme by the corresponding aT, destabilizing the second switch, which eventually self-initiates. However, despite optimization, the switch-to-switch cross-talk remained present in all cases. While digital approaches can, in some cases, mitigate nonspecific effects,[27] in the present situation, a digital duplex approach using an end-point readout is impossible because all compartments containing at least one of the two targets would ultimately exhibit a positive signal in both colors (Figure 1a).

Killer Template Counter Switch Cross-Activation. Solving this problem required a redesign at the circuit level, and we decided to convert the two parallel bistable switches into a tetrastable biochemical circuit. The rationale is that each of the four alternative attracting states can then be attributed to the four possible chemical "states" associated with the presence/absence of each target (0:0, 0:1, 1:0, and 1:1), allowing appropriate classification in each case. To that goal, we designed cross-inhibitory templates (kTs) that connect the two switches bidirectionally (Figure 2). Upon activation by their cognate input (α or β), the kT produces a pT for the opposite switch, thereby acting as a cross-inhibitor of amplification. For the system to admit four states, the inhibitors need to be strong enough to stabilize the state 1:0 and 0:1 (where only one of the two switches is ON), but not too strong to allow the existence of the state 1:1 (where both switches are ON; see mathematical model in Figure S2). Accordingly, we evaluated the effect of the length of the endogenous pT—determined by the length of the deactivating 5′ tail—on the strength of the kT. Figure 3 shows the amplification reaction of a simple β switch in the presence of the α switch triggered using 5 nM of mir39 and an increasing concentration of $\alpha k\beta$ producing various pTβ. The system is set in such a way that, in the absence of $\alpha k\beta$, the β switch turned on spontaneously in around 100 min (Figure S3). When the concentration of kT was increased, we observed, as expected, a growing delay before amplification. Additionally, it is clear that $\alpha k\beta$ producing shorter pTs are stronger inhibitors: less than 100 pM of kT $\alpha k\beta$A1 (meaning that the resulting pTβ will add only one thymidine nucleotide on the 3′ end of the α strand) are required to completely prevent the amplification of the α switch, whereas 100-fold more are needed to observe the same effect with $\alpha k\beta$A4 (Figure 3b). Interestingly, no inhibition was observed in the range of tested concentration for $\alpha k\beta$A5. Similarly, the $\alpha k\beta$A0 (producing a complementary strand from
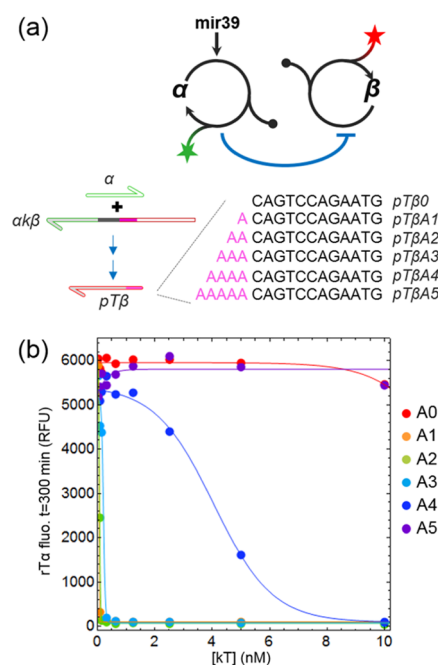

Figure 3. kT efficiency. (a) α-switch, triggered by 5 nM of mir39, is connected to the kT $\alpha k\beta$ producing pTβ of different lengths (with a deactivating tail ranging from 0 to 5 adenylate moieties). (b) Fluorescence of the β switch (t = 300 min) as a function of the concentration of kT.

α with no catalytic extension activity) has no effect on the amplification of the β switch, confirming the catalytic mechanism of the pT. Following these measurements, we opted for kT producing pT with a 4-nucleotide extension, for which the inhibition strength can be easily adjusted by tuning the concentration.

Next, we evaluated the potential of the kT to suppress cross-reactivity between α and β switches, while retaining sensitivity for their cognate target. The two microRNA-sensing circuits are spiked with 0 or 10 pM of mir92a (α switch) and let7a (β switch) in the presence of various concentrations of both $\alpha k\beta$ and $\beta k\alpha$ (Figure 4). Figure 4b,c shows the amplification time of both switches. In these experimental conditions, tetrastability is achieved for 2.5–10 nM of $\beta k\alpha$ and 0.63–1.3 nM of $\alpha k\beta$: in these concentration ranges of the kT, the absence of
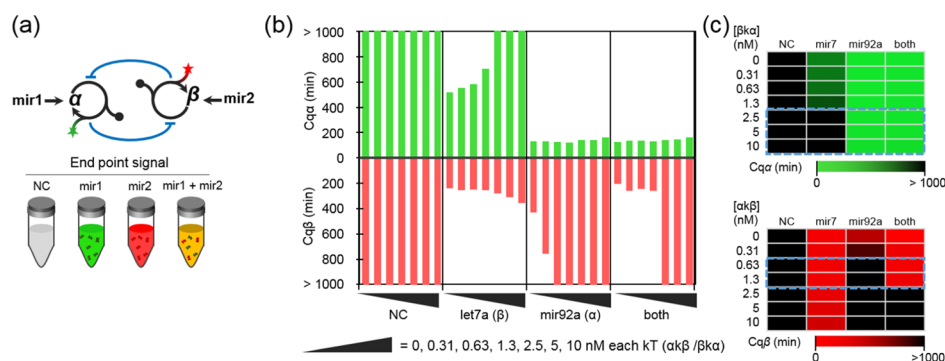
Figure 4. Determination of the kT concentration to suppress cross-activation between the α and β switches. (a) α and β circuits are triggered using 0 or 10 pM of mir92a and let7a, respectively, in the presence of an increasing concentration of αkβ and βkα. (b) Amplification time (Cq) of the α and β switches. (c) Color-coded representation of the Cq as a function of the concentration of the kT. The dashed blue frames represent the concentration of the kT for which the system reaches tetrastability.
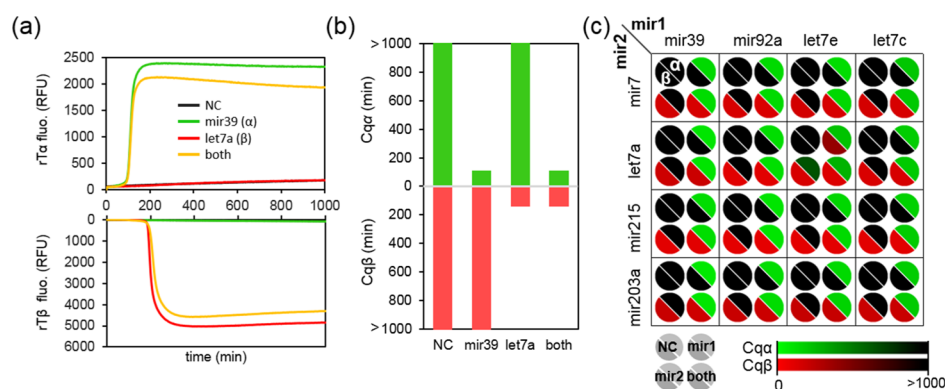

Figure 5. In-solution reprogrammable duplex assay. (a) Amplification curves and (b) extracted Cq of the mir39/let7a duplex assay (0 or 10 pM of mir39 and let7a, associated with α and β switch, respectively). (c) Specificity matrix for 16 different duplex assays. The α switch is associated with mir39, mir92a, let7e, and let7c, and the β switch is connected to mir7, let7a, mir215, and mir203a.
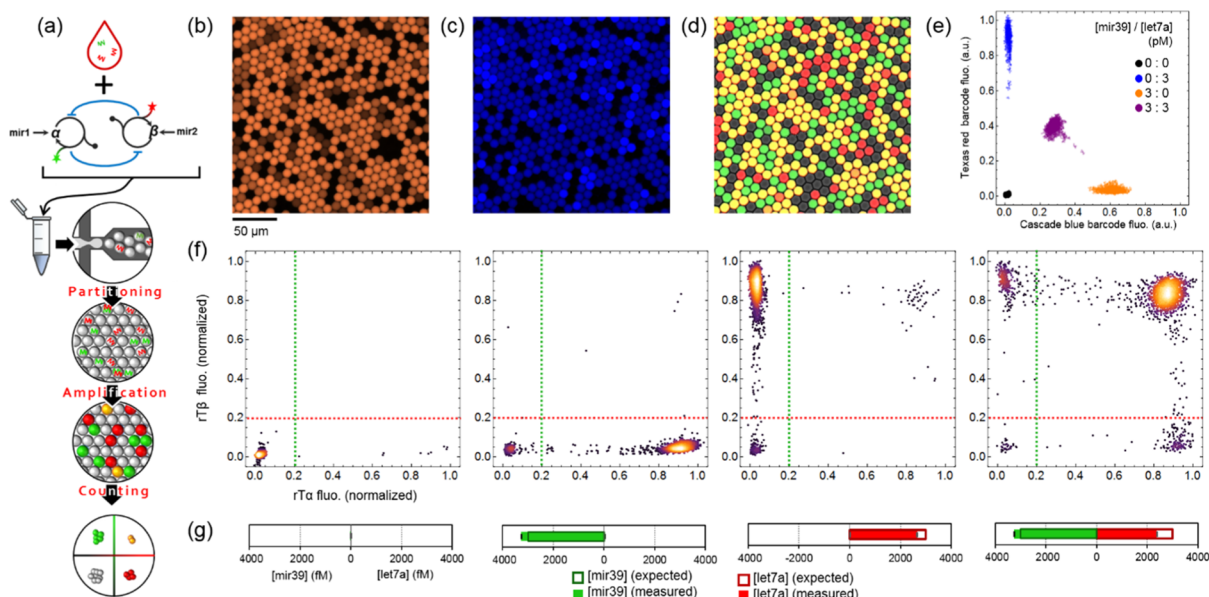

Figure 6. Digital duplex assay. (a) Principle of the digital duplex assay. After emulsifying samples with a microfluidic chip, water-in-oil droplets are incubated and analyzed by microscopy. (b) Microscopy image of the Texas Red and (c) Cascade Blue barcode for the mixture of four droplet populations (0 pM mir39-let7a, 3 pM mir39- 0 pM let7a, 0 pM mir39-3 pM let7a, and 3 pM mir39-let7a). (d) Composite image of the bright-field, red (Atto633 dye) and, green (Oregon green dye) fluorescence. (e) 2D histogram of the barcode intensity of the four color-coded populations. (f) 2D histograms of the probes' fluorescence (α switch = green fluorescence, β switch = red fluorescence). Green and red dashed lines indicate the positive threshold for the α and β switches, respectively. (g) Histograms of the measured vs expected target concentrations.

the target resulted in the absence of amplification (Cq > 1000 min, state 0:0); when only one microRNA target was present, only the corresponding switch amplified a fluorescent signal (Cq ∼ 200 min, states 1:0 and 0:1); finally, when both microRNAs were injected, the two switches turned on (state 1:1).

We tested the generalization of this strategy for the detection of other microRNAs. The modular design of this programmable DNA circuit allows, in principle, the detection of any nucleic acid strand (RNA or DNA), with a known 3′-hydroxyl terminus, by adapting only the converter template's input domain. The rest of the duplex circuit (i.e., both aT, pT, rT, and kT) sequences and concentrations remain untouched. For these experiments, we used eight microRNAs, plugged on either the α switch (cel-mir-39, hsa-mir-92a-5p, hsa-let-7e-5p, and hsa-let-7c-5p) or β switch (hsa-mir-7-5p, hsa-let-7a-5p, hsa-mir215-5p, and hsa-mir203a-3p) (Figure 5). Figure 5c depicts the amplification time (Cq) for the 16 possible duplex experiments in solution for the detection of 0 or 10 pM of microRNA targets (cf. also Figure S4). As expected, the system behaves as a tetrastable biochemical circuit in each case. An exception can be noted for the duplex let7e (α)/let7a (β), where a substantial cross-talk is observed. These two microRNAs differ only by one nucleotide in the ninth position from the 5′ extremity (Figure S4c). Consequently, because the difference in the hybridization enthalpy is low, the two cTs can be activated by either of the two targets, although with a slower kinetic for mismatching targets (which explains that a certain degree of specificity is retained for the duplex detection of these two targets). It can be noted that when let7e is substituted with let7c (which also presents a single base difference with let7a), the corresponding duplex assay is highly specific. This observation can be explained from the fact that the mismatch is located on the fourth position from the 3′ extremity of these microRNAs. This seems enough to impede the polymerase extension on the unmatching cT, preventing unspecific cT activation. At this stage, we confirmed that the cross-inhibitory circuit suppresses unwanted cross-activation, while enabling programmable detection of multiple targets.

Duplex Digital Detection of MicroRNAs. We finally transposed this multiplex assay to a digital readout using droplet microfluidics (Figure 6a). The sample mixture is partitioned into thousands of picoliter-size droplets using a flow-focusing microfluidic device. As a result, target microRNAs are randomly distributed into water-in-oil droplets, with occupancy following a Poissonian distribution. After incubation—which allows the droplet fluorescence to turn either green, red, or both colors (orange) depending on their initial content—the droplets are imaged by epifluorescence microscopy. Knowing the droplet size and the fraction of positive droplets in each color, one can compute back the concentration of the two microRNAs in the original sample (cf. Material and Methods section). We proved that the tetrastable circuit does not significantly alter the amplification time (Figure S5) nor the limit of the blank, in comparison to singleplex assay (Figure S6). As a proof of principle, we prepared four samples spiked with 0 or 3 pM of microRNA mir39 (α switch) and let7a (β switch). Each sample is barcoded with a combination of two fluorescent dextrans and serially emulsified using a homemade sample changer.[35] After incubation, the droplets are imaged by fluorescence microscopy (see the Material and Methods section, Figure 6b−d). While we recorded a few false-positive events, we achieved

accurate quantification of the two microRNAs within 12 ± 6% errors (which could be partially explained by concentration uncertainties from the serial dilution of the targets). In the absence of the kT, we observed a substantial fraction of false-positive events attributed to switch cross-activation (Figure S7). To assess the reproducibility of the technique, we repeated this experiment for samples of different compositions (various concentrations of various microRNAs, see Table S1 of the Supporting Information). For the 30 samples, we observed a good correlation between the expected concentration of the spike-in microRNAs and the measured concentration (Figure 7a). We also verified that the fraction of double-positive
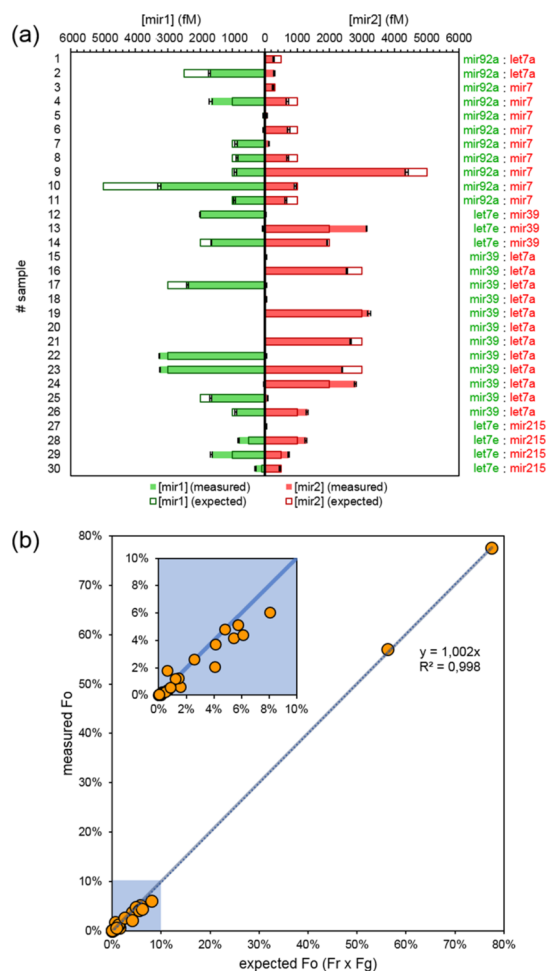

Figure 7. Digital duplex assays of various samples. (a) Analysis of samples of different compositions (microRNA targets and concentrations). (b) Measured percentage of double-positive droplets (F_o) as a function of the expected ratio ($F_g \cdot F_r$), where F_g and F_r correspond to the ratio of green-positive and red-positive droplets, respectively.

droplets (both green and red droplets) corresponds to the fraction expected from the random distribution of the two targets ($F_o = F_g \cdot F_r$, where F_o, F_g, and F_r are the fractions of orange, green, and red droplets) (Figure 7b).

■ CONCLUSIONS

We have introduced a strategy to implement ultrasensitive microRNA detection using isothermal signal amplification in a multiplex, digital format. While isothermal approaches present enticing alternatives to PCR, molecular cross-talks, which may result from limited specificity or from resources sharing, still

present a major challenge. We have previously shown that dynamical molecular circuits, implementing nonlinear functions, can address some of these challenges. For example, a bistable circuit can be used to install ultrasensitivity in DNA-based signal amplification schemes.[28] Here, our approach is built on a tetrastable circuit that stabilizes the two asymmetric ON states necessary for duplex detection and avoids nonspecific response from one target to the other. Our design uses DNA-encoded cross-inhibitors, solving the challenge of balancing the system by having the strength of inhibition reactions controlled by strand concentrations. Using this system, we achieved robust specific amplification in duplex experiments.

In principle, the approach could be extended to detect simultaneously more targets (a triplex assay is shown in Figure S8). However, the direct upscaling of such a network to higher multiplexing would require $n \cdot (n - 1)$ kT and $4 \cdot n$ templates (cT, pT, aT, and rT), where n is the number of targets, which seems arduous beyond $n = 4$. An alternative strategy, avoiding the defavorable accumulation of templates, could use generic inhibitors, where triggered switches forbid the start of all untriggered ones using a universal pathway. Such a "winners-take-all" approach would limit the number of kTs to n, allowing a higher level of multiplexing (Figure S9).[33,36]

Here, as a proof of principle, we implemented a duplex assay for the codetection of two microRNA targets. We demonstrated that the tetrastable DNA circuit can be adapted for the digital detection of microRNAs, providing absolute, calibration-free quantification for a variety of target pairs. The digitalization of this duplex assay is possible, first, because the DNA circuit is sensitive enough to amplify the signal from a single target molecule, isolated in picoliter-sized compartments; second because kT inhibitors prevent nonspecific amplification caused by cross-talk reactivity. Possible applications of the duplex assay in the microRNA quantification approach can include measuring simultaneously up- and down-regulated targets or including a "housekeeping" or spiked target as internal control in biomarker measurements.

■ MATERIALS AND METHODS

Materials. HPLC-purified oligonucleotides were purchased from Biomers or Eurofins and resuspended at 100 μM in 1× tris−EDTA at pH 7.5 for long-term storage. The nicking enzymes Nb.BsmI and Nt.bstNBI, the restriction enzyme BsmI, the DNA polymerase Vent(exo-), BSA, and dNTP were obtained from New England Biolabs (NEB). *Thermus thermophilus* RecJ exonuclease was produced in-house by following a previously published protocol.[37] Sodium chloride, potassium chloride, magnesium sulfate, ammonium sulfate, Trizma hydrochloride, netropsin, and synperonic F104 were purchased from Merck (Sigma-Aldrich).

Template Design. Templates were designed according to the rules described elsewhere.[28,32,38] Template sequences aT, pT, rT, and kT were protected against the 5′ → 3′ exonuclease activity of ttRecJ by the addition of three 5′ phosphorothioate backbone modifications. Templates aT, pT, cT, and kT were blocked to prevent unwanted polymerization by the addition of a 3′ phosphate moiety. aTs were designed to hybridize only the last 10 bases of corresponding inputs (α or β) in order to favor the deactivation by the pT of signal strands produced by the leaky reaction.[32] kTs present the same shortened input binding site in order to reduce the competitive binding of signal strands. This prevents the nonspecific activation of the kT prior to target-triggered amplification. Table S2 recapitulates all sequences used throughout this study.

Reaction Mixture Assembly. All reaction mixtures were assembled at 4 °C in 200 μL PCR tubes. Template and enzymes

were first mixed with the reaction buffer (20 mM Tris-HCl, pH 8.9, 10 mM $(NH_4)_2SO_4$, 40 mM KCl, 10 mM $MgSO_4$, 50 μM each dNTP, 0.1% (w/v) synperonic F104, 2 μM netropsin, and 200 μg/mL BSA). Optimized template concentrations were as follows: aTα = 50 nM, aTβ, 50 nM, pTα = 15 nM, pTβ = 11 nM, rTα = 40 nM, rTβ = 40 nM, cT (each) = 0.5 nM, αkβ = 1 nM, and βkα = 2.5 nM. Enzyme concentrations were Nb.BsmI = 300 u/mL, Nt.BstNBI = 10 u/mL, Vent(exo-) = 60 u/mL, BsmI = 60 u/mL, and ttRecJ = 23 nM. After homogenization, samples were spiked with microRNA solution, itself serially diluted in 1× tris−EDTA buffer using low-bind DNA tips (Eppendorf). Samples (bulk or emulsion) were incubated at 50 °C in a qPCR machine CFX96 touch (Bio-Rad).

Microfluidic Droplet Generation. A two-inlet flow-focusing device was prepared using standard soft-lithography techniques. In brief, the microfluidic mold was obtained by coating a 4 in. silicon wafer with SU-8 photoresist (MicroChem Corp.) reticulated upon UV exposure. Following careful cleaning of the mold using isopropanol, a 10:1 mixture of Sylgard 184 polydimethylsiloxane (PDMS) resin (40 g)/curing agent (4 g) (Dow Corning) was poured onto the mold, degassed under vacuum, and baked for 2 h at 70 °C. The PDMS slab was peeled off the mold, and inlets and outlets were punched using a 1.5 mm diameter biopsy puncher (Integra Miltex). The PDMS slab was bound on a 1 mm thick glass slide (Paul Marienfeld GmbH & Co) immediately following oxygen plasma activation. The chip underwent baking for 5 h at 200 °C to make the channel hydrophobic. Monodisperse water-in-oil droplets were generated by mixing the aqueous samples and the continuous phase (fluorinated oil Novec 7500, 3 M + 1% (w/w) fluorosurf, Emulseo) on the chip using a pressure pump controller MFCS-EZ (Fluigent) and 200 μm inner diameter polytetrafluoroethylene tubing (C.I.L.).

Droplet Imaging and Analysis. Following incubation, emulsions were imaged by microscopy. A monolayer of droplets was sandwiched between two glass slides (1 mm thick bottom slide, Paul Marienfeld GmbH & Co, 0.17 mm thick top slide, VWR) spaced using 10 μm polystyrene particles (Polysciences, Inc.) to avoid droplet compression. The chamber was sealed with epoxy glue (Sader). Images were acquired on an epifluorescence microscope Eclipse Ti equipped with a motorized XY stage (Nikon), a camera Nikon DS-Qi2, an apochromatic 10× objective (N.A. 0.45, Nikon) and a CoolLed pE-400 illumination source. Composite images were generated with the open source software ImageJ. Droplets were analyzed using the Mathematica software (Wolfram) by following a previously reported procedure.[28] The concentration of microRNA is computed using the formula

$$[\text{mir1}] = \frac{-\ln(1 - F_g)}{N_A \cdot V}$$

and

$$[\text{mir2}] = \frac{-\ln(1 - F_r)}{N_A \cdot V}$$

where F_g and F_r are the fraction of green- and red-positive droplets, respectively; N_A is the Avogadro number, and V is the volume of the droplets.

■ ASSOCIATED CONTENT

Ⓢ Supporting Information

The Supporting Information is available free of charge at https://pubs.acs.org/doi/10.1021/acssensors.0c00593.

> Nb.BsmI effect on the self-start, extended data from Figure 3, extended data from Figure 5c, in-solution singleplex versus duplex assay, limit of the blank single versus duplex assay, digital duplex assay in the absence of the kT, mathematical model of the duplex network, digital triplex assay, scaling-up strategies for multiplex digital assays, oligonucleotide sequences, and raw data from duplex digital analysis (PDF)

AUTHOR INFORMATION

Corresponding Author

Guillaume Gines − *Gulliver Laboratory, ESPCI Paris—Université PSL, 75005 Paris, France;* ◉ orcid.org/0000-0003-1012-3250; Phone: (33)1-40-79-58-51; Email: guillaume.gines@espci.fr

Author

Yannick Rondelez − *Gulliver Laboratory, ESPCI Paris—Université PSL, 75005 Paris, France;* ◉ orcid.org/0000-0002-2565-476X

Complete contact information is available at:
https://pubs.acs.org/10.1021/acssensors.0c00593

Author Contributions

Both authors conceived the study and wrote the manuscript. G.G. performed the experiments.

Notes

The authors declare no competing financial interest.

REFERENCES

(1) Zhao, Y.; Chen, F.; Li, Q.; Wang, L.; Fan, C. Isothermal Amplification of Nucleic Acids. *Chem. Rev.* **2015**, *115*, 12491−12545.

(2) Jonstrup, S. P.; Koch, J.; Kjems, J. A MicroRNA Detection System Based on Padlock Probes and Rolling Circle Amplification. *RNA* **2006**, *12*, 1747−1752.

(3) Zhao, W.; Ali, M. M.; Brook, M. A.; Li, Y. Rolling Circle Amplification: Applications in Nanotechnology and Biodetection with Functional Nucleic Acids. *Angew. Chem., Int. Ed.* **2008**, *47*, 6330−6337.

(4) Notomi, T.; Mori, Y.; Tomita, N.; Kanda, H. Loop-Mediated Isothermal Amplification (LAMP): Principle, Features, and Future Prospects. *J. Microbiol.* **2015**, *53*, 1−5.

(5) Toley, B. J.; Covelli, I.; Belousov, Y.; Ramachandran, S.; Kline, E.; Scarr, N.; Vermeulen, N.; Mahoney, W.; Lutz, B. R.; Yager, P. Isothermal Strand Displacement Amplification (ISDA): A Rapid and Sensitive Method of Nucleic Acid Amplification for Point-of-Care Diagnosis. *Analyst* **2015**, *140*, 7540−7549.

(6) Walker, G. T.; Fraiser, M. S.; Schram, J. L.; Little, M. C.; Nadeau, J. G.; Malinowski, D. P. Strand Displacement Amplification−an Isothermal, in Vitro DNA Amplification Technique. *Nucleic Acids Res.* **1992**, *20*, 1691−1696.

(7) Zhou, W.; Hu, L.; Ying, L.; Zhao, Z.; Chu, P. K.; Yu, X.-F. A CRISPR−Cas9-Triggered Strand Displacement Amplification Method for Ultrasensitive DNA Detection. *Nat. Commun.* **2018**, *9*, 5012.

(8) Li, J.; Macdonald, J.; von Stetten, F. Review: A Comprehensive Summary of a Decade Development of the Recombinase Polymerase Amplification. *Analyst* **2018**, *144*, 31−67.

(9) Wee, E. J. H.; Trau, M. Simple Isothermal Strategy for Multiplexed, Rapid, Sensitive, and Accurate MiRNA Detection. *ACS Sens.* **2016**, *1*, 670−675.

(10) Reid, M. S.; Le, X. C.; Zhang, H. Exponential Isothermal Amplification of Nucleic Acids and Assays for Proteins, Cells, Small Molecules, and Enzyme Activities: An EXPAR Example. *Angew. Chem., Int. Ed.* **2018**, *57*, 11856−11866.

(11) Jarvius, J.; Melin, J.; Göransson, J.; Stenberg, J.; Fredriksson, S.; Gonzalez-Rey, C.; Bertilsson, S.; Nilsson, M. Digital Quantification Using Amplified Single-Molecule Detection. *Nat. Methods* **2006**, *3*, 725−727.

(12) Yuan, H.; Chao, Y.; Shum, H. C. Droplet and Microchamber-Based Digital Loop-Mediated Isothermal Amplification (DLAMP). *Small* **2020**, *16*, 1904469.

(13) Shen, F.; Davydova, E. K.; Du, W.; Kreutz, J. E.; Piepenburg, O.; Ismagilov, R. F. Digital Isothermal Quantification of Nucleic Acids via Simultaneous Chemical Initiation of Recombinase Polymerase Amplification Reactions on SlipChip. *Anal. Chem.* **2011**, *83*, 3533−3540.

(14) Muñoz, H. E.; Riche, C. T.; Kong, J. E.; van Zee, M.; Garner, O. B.; Ozcan, A.; Di Carlo, D. Fractal LAMP: Label-Free Analysis of Fractal Precipitate for Digital Loop-Mediated Isothermal Nucleic Acid Amplification. *ACS Sens.* **2020**, *5*, 385−394.

(15) Schuler, F.; Schwemmer, F.; Trotter, M.; Wadle, S.; Zengerle, R.; von Stetten, F.; Paust, N. Centrifugal step emulsification applied for absolute quantification of nucleic acids by digital droplet RPA. *Lab Chip* **2015**, *15*, 2759−2766.

(16) Chapin, S. C.; Appleyard, D. C.; Pregibon, D. C.; Doyle, P. S. Rapid MicroRNA Profiling on Encoded Gel Microparticles. *Angew. Chem., Int. Ed.* **2011**, *50*, 2289−2293.

(17) Geiss, G. K.; Bumgarner, R. E.; Birditt, B.; Dahl, T.; Dowidar, N.; Dunaway, D. L.; Fell, H. P.; Ferree, S.; George, R. D.; Grogan, T.; James, J. J.; Maysuria, M.; Mitton, J. D.; Oliveri, P.; Osborn, J. L.; Peng, T.; Ratcliffe, A. L.; Webster, P. J.; Davidson, E. H.; Hood, L.; Dimitrov, K. Direct Multiplexed Measurement of Gene Expression with Color-Coded Probe Pairs. *Nat. Biotechnol.* **2008**, *26*, 317−325.

(18) Roy, S.; Soh, J. H.; Ying, J. Y. A Microarray Platform for Detecting Disease-Specific Circulating MiRNA in Human Serum. *Biosens. Bioelectron.* **2016**, *75*, 238−246.

(19) Nallur, G.; Luo, C.; Fang, L.; Cooley, S.; Dave, V.; Lambert, J.; Kukanskis, K.; Kingsmore, S.; Lasken, R.; Schweitzer, B. Signal Amplification by Rolling Circle Amplification on DNA Microarrays. *Nucleic Acids Res.* **2001**, *29*, No. e118.

(20) Traeger, J. C.; Schwartz, D. K. Surface-Mediated DNA Hybridization: Effects of DNA Conformation, Surface Chemistry, and Electrostatics. *Langmuir* **2017**, *33*, 12651−12659.

(21) Kunze, A.; Dilcher, M.; Abd El Wahed, A.; Hufert, F.; Niessner, R.; Seidel, M. On-Chip Isothermal Nucleic Acid Amplification on Flow-Based Chemiluminescence Microarray Analysis Platform for the Detection of Viruses and Bacteria. *Anal. Chem.* **2016**, *88*, 898−905.

(22) McDermott, G. P.; Do, D.; Litterst, C. M.; Maar, D.; Hindson, C. M.; Steenblock, E. R.; Legler, T. C.; Jouvenot, Y.; Marrs, S. H.; Bemis, A.; Shah, P.; Wong, J.; Wang, S.; Sally, D.; Javier, L.; Dinio, T.; Han, C.; Brackbill, T. P.; Hodges, S. P.; Ling, Y.; Klitgord, N.; Carman, G. J.; Berman, J. R.; Koehler, R. T.; Hiddessen, A. L.; Walse, P.; Bousse, L.; Tzonev, S.; Hefner, E.; Hindson, B. J.; Cauly, T. H.; Hamby, K.; Patel, V. P.; Regan, J. F.; Wyatt, P. W.; Karlin-Neumann, G. A.; Stumbo, D. P.; Lowe, A. J. Multiplexed Target Detection Using DNA-Binding Dye Chemistry in Droplet Digital PCR. *Anal. Chem.* **2013**, *85*, 11619−11627.

(23) Didelot, A.; Kotsopoulos, S. K.; Lupo, A.; Pekin, D.; Li, X.; Atochin, I.; Srinivasan, P.; Zhong, Q.; Olson, J.; Link, D. R.; Laurent-Puig, P.; Blons, H.; Hutchison, J. B.; Taly, V. Multiplex Picoliter-Droplet Digital PCR for Quantitative Assessment of DNA Integrity in Clinical Samples. *Clin. Chem.* **2013**, *59*, 815.

(24) Qiu, X.; Guo, J.; Xu, J.; Hildebrandt, N. Three-Dimensional FRET Multiplexing for DNA Quantification with Attomolar Detection Limits. *J. Phys. Chem. Lett.* **2018**, *9*, 4379−4384.

(25) Marras, S. A. E.; Tyagi, S.; Antson, D.-O.; Kramer, F. R. Color-Coded Molecular Beacons for Multiplex PCR Screening Assays. *PLoS One* **2019**, *14*, No. e0213906.

(26) Zhong, Q.; Bhattacharya, S.; Kotsopoulos, S.; Olson, J.; Taly, V.; Griffiths, A. D.; Link, D. R.; Larson, J. W. Multiplex Digital PCR: Breaking the One Target per Color Barrier of Quantitative PCR. *Lab Chip* **2011**, *11*, 2167−2174.

(27) Whale, A. S.; Huggett, J. F.; Tzonev, S. Fundamentals of Multiplexing with Digital PCR. *Biomol. Detect. Quantif.* **2016**, *10*, 15−23.

(28) Gines, G.; Menezes, R.; Nara, K.; Kirstetter, A.-S.; Taly, V.; Rondelez, Y. Isothermal Digital Detection of MicroRNA Using Background-Free Molecular Circuit. *Sci. Adv.* **2020**, *6*, No. eaay5952.

(29) Qian, J.; Ferguson, T. M.; Shinde, D. N.; Ramírez-Borrero, A. J.; Hintze, A.; Adami, C.; Niemz, A. Sequence Dependence of Isothermal DNA Amplification via EXPAR. *Nucleic Acids Res.* **2012**, *40*, No. e87.

(30) Tan, E.; Erwin, B.; Dames, S.; Ferguson, T.; Buechel, M.; Irvine, B.; Voelkerding, K.; Niemz, A. Specific versus Nonspecific Isothermal DNA Amplification through Thermophilic Polymerase and Nicking Enzyme Activities. *Biochemistry* **2008**, *47*, 9987−9999.

(31) Jia, H.; Li, Z.; Liu, C.; Cheng, Y. Ultrasensitive Detection of MicroRNAs by Exponential Isothermal Amplification. *Angew. Chem., Int. Ed.* **2010**, *49*, 5498−5501.

(32) Montagne, K.; Gines, G.; Fujii, T.; Rondelez, Y. Boosting Functionality of Synthetic DNA Circuits with Tailored Deactivation. *Nat. Commun.* **2016**, *7*, 13474.

(33) Genot, A. J.; Fujii, T.; Rondelez, Y. Scaling down DNA Circuits with Competitive Neural Networks. *J. R. Soc., Interface* **2013**, *10*, 20130212.

(34) Genot, A. J.; Fujii, T.; Rondelez, Y. Computing with Competition in Biochemical Networks. *Phys. Rev. Lett.* **2012**, *109*, 208102.

(35) Menezes, R.; Dramé-Maigné, A.; Taly, V.; Rondelez, Y.; Gines, G. Streamlined Digital Bioassays with a 3D Printed Sample Changer. *Analyst* **2019**, *145*, 572−581.

(36) Cherry, K. M.; Qian, L. Scaling up Molecular Pattern Recognition with DNA-Based Winner-Take-All Neural Networks. *Nature* **2018**, *559*, 370.

(37) Yamagata, A.; Masui, R.; Kakuta, Y.; Kuramitsu, S.; Fukuyama, K. Overexpression, Purification and Characterization of RecJ Protein from Thermus Thermophilus HB8 and Its Core Domain. *Nucleic Acids Res.* **2001**, *29*, 4617−4624.

(38) Baccouche, A.; Montagne, K.; Padirac, A.; Fujii, T.; Rondelez, Y. Dynamic DNA-Toolbox Reaction Circuits: A Walkthrough. *Methods* **2014**, *67*, 234−249.